International Communications in Heat and Mass Transfer 117 (2020) 104800

Contents lists available at ScienceDirect

International Communications in Heat and Mass Transfer

journal homepage: www.elsevier.com/locate/ichmt

Enhancing and attenuating heat transfer characteristics for circulating flows of nanofluids within rectangular enclosures

Bin Wang[a,*], Tien-Mo Shih[b], Jiping Huang[a,*]

[a] Department of Physics, State Key Laboratory of Surface Physics, Key Laboratory of Micro and Nano Photonic Structures (MOE), Fudan University, Shanghai 200433, China

[b] Department of Mechanical Engineering, University of California, Berkeley, CA 94720, USA

ARTICLE INFO

Keywords:
Nanofluids
Nusselt number
Heat-transfer attenuating
Heat-transfer enhancing
Mildly zigzag
COMSOL

ABSTRACT

Due to wide applications of nanofluids to designs of thermal engineering systems, the free convection participated by nanofluids inside rectangular enclosures has been intensively investigated. Generally, rightward-traveling heat transfer across a rectangular enclosure is enhanced when a pure base fluid is replaced with a nanofluid. Amid numerous dedicated literature studies of such a phenomenon, a somewhat anomalous behavior for at least four types of nanofluids has been unreported. Here we have numerically discovered this behavior in terms of averaged Nusselt number versus the nanoparticle volume fraction parameterized in enclosure-geometry Aspect ratio and Rayleigh number. At $AR \geq 2.5$ and $Ra = 10^4$, a regime, in which the average Nusselt number may enhance or diminish as the nanoparticle volume fraction increases, has unexpectedly emerged. Furthermore, as the aspect ratio increases, the average Nusselt number features mildly zigzag performances at large Rayleigh numbers. Being validated with simulation results, mechanisms that govern the emergence of such phenomena are also identified. Our study may benefit future investigations that desire to understand heat-transfer mechanisms of nanofluids and to optimize heat-transfer characteristics for various thermal systems.

1. Introduction

Natural convection heat transfer in enclosures has been investigated for a wide variety of technological applications, such as solar collectors, home ventilation, fire prevention, reactor insulation, power plant among others. Different subjects of free convection heat transfer in rectangular cavities have been investigated thoroughly [1–5]. In general, conventional heat transfer fluids, such as water, ethylene glycol, and engine oil, render unsatisfactory cooling effects due to the limitation of their thermal-conductivity values in comparison with those of liquid metals. However, even though liquid metals thermally conduct well, they also cost highly. Nanofluids, first studied by Choi [6], appears as an appropriate candidate,satisfying both criteria of the thermal conductivity and the cost [7]. Therefore, several investigators reported that up to 20% heat transfer enhancement could be achieved simply using low volume fractions of nanoparticles (e.g. 1 % ~ 5%) [8–10], prompting further research interests.

In parallel, the understanding of flow behaviors within enclosures is recently regarded as one of fundamental concerns, and hence problems has been ensued extensively [11–16]. Khanafer et al. [17] conducted numerical studies on free convection inside nanofluid right wall, hot left wall and insulated horizontal walls. Their results as well as similar ones obtained by Jou and Tseng [18] showed that, for the entire range of Rayleigh number (*Ra*) considered, the rate of heat transfer increased with an increase in nanoparticle volume fractions. Influences due to uncertainties in the effective dynamic viscosity and the thermal conductivity of alumina-water nanofluids on free convection heat transfer in a differentially heated square cavity were investigated by Ho et al. [19]. The obtained results demonstrated that the heat transfer across the cavity could be enhanced with respect to the base fluid and the dynamic viscosity formulation. Oztop and Abu-nada [20] carried out numerical studies on free convection of nanofluids within partially heated rectangular cavities, which consisted of a cold vertical wall, a localized heater on the other vertical wall, and insulated horizontal walls. Effects of Rayleigh number, aspect ratio of cavities, size and location of the heater and different types of water-based nanofluids were considered. It was found that the average Nusselt number increased with an increase in the volume fraction of nanoparticles and heights of heaters. Free convection heat transfer of water-based nanofluids in an inclined square cavity was studied numerically by Ogut [21]. In their work, average heat transfer rates increased significantly as particle volume fractions and Rayleigh numbers increased. Sheikhzadeh et al.

* Corresponding authors.
E-mail addresses: onebeingbeing@126.com (B. Wang), jphuang@fudan.edu.cn (J. Huang).

https://doi.org/10.1016/j.icheatmasstransfer.2020.104800

Nomenclature

ΔT	difference temperature between hot wall and cold wall $=T_h - T_c$
AR	aspect ratio $=L/H$
c_p	specific heat capacity with pressure kept constant $J/(kg \cdot K)$
g	gravitational acceleration (m/s^2)
H	height of the rectangular enclosure (m)
h	local heat transfer coefficient $(W/(m^2K))$
k	thermal conductivity $(W/(m \cdot K))$
L	length of the rectangular enclosure (m)
Nu	average Nusselt number $=hH/k$
p	pressure (Pa)
Pr	Prandtl number $=\nu_f/\alpha_f$
Q_{cd}	integrated conductive flow (W/m)
Q_{cv}	integrated convective flow (W/m)
Q_T	integrated total energy flow (W/m)
Ra	Rayleigh number $=g\beta_f H^3 \Delta T/(\nu_f \alpha_f)$
T	temperature (K)
u	x-direction velocity (m/s)
v	y-direction velocity (m/s)
v_{max}	maximum velocity in y direction (m/s)
X	dimensionless x-coordinate $=x/H$
x	x coordinate (m)
y	y coordinate (m)

Greek symbols

α	thermal diffusivity (m^2/s)
β	thermal expansion coefficient $(1/K)$
μ	viscosity $(kg/(m \cdot s))$
ν	kinematic viscosity (m^2/s)
ϕ	nanoparticle volume fraction
ρ	density (kg/m^3)
θ	dimensionless temperature $=(T - T_c)/\Delta T$

Subscript

c	cold
f	fluid
h	hot
l	local
nf	nanofluid
s	solid

[22] conducted a numerical simulation to study free convection of *Cu*-water nanofluid inside a square cavity with partially thermally active sidewalls, and found that maximum average Nusselt number (*Nu*) for high *Ra* occurred when hot and cold parts were located in the bottom and middle region of vertical walls, respectively. Analyzing free convection of nanofluid in a differentially heated square cavity using a single-phase thermal dispersion model, Kumar et al. [23] inferred that the average *Nu* increased with the solid volume fraction. Saidi et al. [24] investigated *Cu*-water nanofluid inside L-shaped enclosures, and reported an augmentation in heat transfer with an increment percentage of the suspended nanoparticles at any given Grashof number (*Gr*) or Rayleigh number (*Ra*). However, contradictory experimental findings were reported by Putra et al. [25] using Al_2O_3 and *CuO* water nanofluids. These investigators found that the heat transfer coefficient was lower than that for a pure fluid. Santra et al. [26] studied free convection of *Cu*-water nanofluid in a differentially heated square cavity with the assumption of Ostwaldede Waele non-Newtonian nanfluid behaviors. They found that rates of heat transfer decreased when nanoparticle volume fractions increased for a particular *Ra*. In numerical studies examining free convection of Al_2O_3-water nanofluid in a differentially heated cavity with consideration of slip mechanism in nanofluids, Lin and Violi [27] found enhanced or mitigated heat transfer effects due to the presence of nanoparticles. Sheikhzadeh et al. [28] numerically investigated the problem of free convection of the TiO_2-water nanofluid in rectangular cavities differentially heated on adjacent walls. They found that, by increasing in the volume fraction of nanoparticles, the mean *Nu* of the hot wall increased for shallow cavities while the reverse trend occurred for tall cavities. Free convection of the Al_2O_3-water and the *CuO*-water nanofluids in a square cavity using nanoparticles volume fraction and temperature-dependent viscosity and thermal conductivity relationships [29,30] was numerically studied Abu-nada et al. [31], who compared the aforementioned model with Brinkman model [32] for the dynamic viscosity and did the aforementioned model with Maxwell model [33] for the thermal conductivity. They concluded that, at high *Ra*, the heat transfer rate was sensitive to the viscosity model while thermal conductivity model did not influence on heat transfer rate. Moreover, another experimental work in natural convection conducted by Wen and Ding [34] highlighted deterioration in heat transfer by the addition of nanoparticles. Numerous works investigating the square enclosure ($AR = 1$) show heat transfer enhancement monotonously growth with concentration of nanofluids. In recent years, numerous comprehensive reviews [35–38] reported heat transfer characteristics of nanofluids under different conditions. Numerous researchers [20,24,31,39,40] showed that the aspect ratio may exert a great impact on heat transfer enhancement. However, even though a great number of investigations were dedicated to nanofluids heat transfer in rectangular enclosure, the systematic relation between Nusselt number and aspect ratio on nanofluids remains lacking. The present study attempts to join these investigators' laborious and remarkable efforts with its emphasis on the average-Nusselt-number (*Nu*) optimization in terms of three critical parameters, namely, Rayleigh number (*Ra*), aspect ratio ($AR = L/H$), and the volume fraction of nanoparticles (ϕ) for four different materials (*Ag*, *Cu*, Al_2O_3, TiO_2). In particular, we have (1) discovered two opposing heat transfer phenomena and zigzag heat transfer phenomena, as well as (2) explained mechanisms that govern these phenomena.

2. Modeling

2.1. Problem definition

As shown in the system schematic (Fig. 1), the nanofluid, composed of water and solid spherical nanoparticles, recirculates in the enclosure with height H and width L, subject to boundary conditions prescribed as constant T_h and T_c maintained for two vertical sides and insulation for top and bottom sides. A few idealizations have been made:

a) particles are manufactured unifyingly in sizes and shapes (sphere);

b) the base fluid, namely water, and solid spherical nanoparticles are mixed so thoroughly that the mixture can be treated as a pure substance;

c) the behavior of flow is Newtonian;

d) k_{nf} and μ_{nf} are prescribed by pre-determined functions of ϕ, k_f, k_s, and μ_f [32,33].

Our focus lies on flow characteristics affected by four parameters: nanoparticles, volume fraction of nanofluids, aspect ratio, and Rayleigh number which are partly determined by properties listed in Table 1.

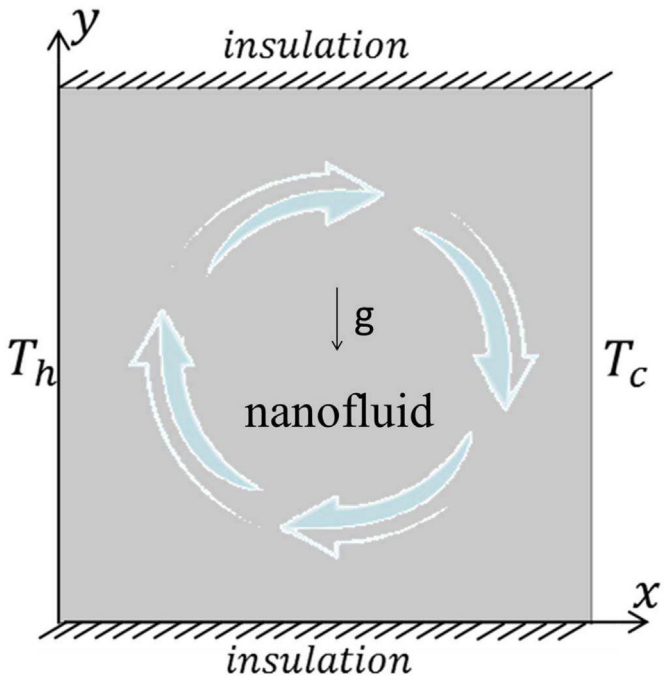

Fig. 1. System schematic. Nanofluids recirculate in the enclosure with height H and width L, subject to boundary conditions prescribed as constant T_h and T_c maintained for two vertical sides and insulation for top and bottom sides. The gravitational force is aligned negatively in the y direction.

Table 1
Thermophysical properties of water, *Ag*, *Cu*, Al_2O_3 and TiO_2 at 20°C [20,41].

Physical properties	Fluid phase	*Ag*	*Cu*	Al_2O_3	TiO_2
$c_p(J/kg \cdot K)$	4179	235	385	765	686.2
$\rho(kg/m^3)$	997.1	10500	8933	3970	4250
$k(W/m \cdot K)$	0.613	429	401	40	8.95
$\beta \times 10^5(1/K)$	21	1.89	1.67	0.85	0.9
$\alpha \times 10^7(m^2/s)$	1.47	1738.6	1163.1	131.7	30.7

2.2. Mathematical model

Partial differential equations governing steady-state mass conservation, momentum transports, and energy transport can be written as

$$\frac{\partial \rho_{nf} u}{\partial x} + \frac{\partial \rho_{nf} v}{\partial y} = 0, \tag{1}$$

$$\frac{\partial \rho_{nf} u^2}{\partial x} + \frac{\partial \rho_{nf} uv}{\partial y} = -\frac{\partial p}{\partial x} + \mu_{nf}\left(\frac{\partial^2 u}{\partial x^2} + \frac{\partial^2 u}{\partial y^2}\right), \tag{2}$$

$$\frac{\partial \rho_{nf} vu}{\partial x} + \frac{\partial \rho_{nf} v^2}{\partial y} = -\frac{\partial p}{\partial y} + \mu_{nf}\left(\frac{\partial^2 v}{\partial x^2} + \frac{\partial^2 v}{\partial y^2}\right) - \rho_{nf} g, \tag{3}$$

$$\frac{\partial \rho_{nf} uT}{\partial x} + \frac{\partial \rho_{nf} vT}{\partial y} = \rho_{nf}\alpha_{nf}\left(\frac{\partial^2 T}{\partial x^2} + \frac{\partial^2 T}{\partial y^2}\right), \tag{4}$$

where effective properties for the nanofluid, ρ_{nf} and α_{nf}, are defined as

$$\rho_{nf} = \rho_{nfc}(1 - \beta_{nf}(T - T_c)), \tag{5}$$

$$\rho_{nfc} = (1 - \phi)\rho_f + \phi\rho_s, \tag{6}$$

and

$$\alpha_{nf} = k_{nf}/(\rho C_p)_{nf}. \tag{7}$$

The thermal expansion coefficient of the nanofluid is determined by

$$\beta_{nf} = (1 - \phi)\beta_f + \phi\beta_s. \tag{8}$$

Here additional effective properties required for the analysis include the heat capacitance of the nanofluid given as [42].

$$(\rho C_p)_{nf} = (1 - \phi)(\rho C_p)_f + \phi(\rho C_p)_s, \tag{9}$$

The Brinkman correlation [32].

$$\mu_{nf} = \frac{\mu_f}{(1 - \phi)^{2.5}} \tag{10}$$

can be used to calculate the effective dynamic viscosity of the nanofluid.

The nanofluid thermal conductivity can be calculated according to Maxwell equation [33] as

$$k_{nf} = k_f \frac{(k_s + 2k_f) - 2\phi(k_f - k_s)}{(k_s + 2k_f) + \phi(k_f - k_s)}, \tag{11}$$

where k_s and k_f are the thermal conductivity of dispersed nanoparticles and pure water, respectively.

The Rayleigh number for problems involving nanofluids is defined as

$$Ra = \frac{g\beta_f H^3 \Delta T}{\nu_f \alpha_f}. \tag{12}$$

The average Nusselt number is determined by:

$$Nu = \frac{1}{H}\int_0^H Nu_l(y)\mathrm{d}y. \tag{13}$$

where the local Nusselt number can be expressed as

$$Nu_l = \frac{hH}{k_f}. \tag{14}$$

Heat transfer coefficient are calculated from the following equation,

$$h = \frac{-k_{nf}}{T_h - T_c}\frac{\partial T}{\partial x}, \; on \;\; the \;\; vertical \;\; walls. \tag{15}$$

By substituting Eq. (15) into Eq. (14), the local Nusselt number can be written as

$$Nu_l = -\frac{k_{nf}}{k_f}\frac{\partial \theta}{\partial X}, \; on \;\; the \;\; vertical \;\; walls. \tag{16}$$

Governing equations. (1–4) along with Eqs. (5–11) are used for simulations, whereas Eqs. (12–16) are adopted for post-processing purposes.

3. Numerical method and validation

The commercial package (COMSOL) [46] is used to solve Eqs. (1–4). The algorithm in COMSOL is based on the Galerkin finite element method. Detail narratives of the Galerkin finite element method can be found in Refs. [47–49], because our attention is focused on analyses of thermal physics.

For the model validation, numerical results are compared with the literature data, and satisfactory agreement has been achieved (Table 2)

Table 2
Comparison of the average Nusselt number in an air filled rectangular enclosure at $AR = 1$ [17,31,43–45].

	$Ra = 10^3$	$Ra = 10^4$	$Ra = 10^5$	$Ra = 10^6$
Khanafer et al. [17]	1.118	2.245	4.522	8.826
Abu-Nada et al. [31]	1.120	2.244	4.644	8.862
De Vahl Davis and Jones [43]	1.118	2.243	4.52	8.799
Barakos and Mistoulis [44]	1.114	2.245	4.51	8.806
Fusegi et al. [45]	1.105	2.23	4.646	9.012
Present work	1.122	2.261	4.553	8.885

[17,31,43–45].

4. Results and discussion

In the present study, we emphasize on effects of ϕ, Ra, AR, and material types on the heat transfer rate.

The Nu values in enclosures with four types of nanofluids parameterized by Ra and ϕ at $AR = 1.5$ are presented in Fig. 2. For the same nanofluid, and in the entire range of Ra values, Nu increases monotonically with increasing ϕ. For the same nanofluid, at a fixed ϕ, Nu increases as Ra increases, as expected. On the other hand, the trend for $AR < 1.5$ looks quite similar with that of $AR = 1.5$ exhibited in these four sub-figures, as confirmed by that of $AR = 1$ in Ref. [20].

For comparison, Nu values in enclosures with four types of nanofluids parameterized by Ra and ϕ at $AR = 4$ are presented in Fig. 3. For the same nanofluid, as well as at $Ra = 10^3$, 10^5, and 10^6, Nu increases monotonically with increasing ϕ. At this juncture, we wish to present the case $Ra = 10^4$ ($AR = 4$ and four different nanofluids), in which Nu results exhibit interesting behaviors, constituting the crux of the present analysis. For Ag and Cu, Nu conspicuously increases as ϕ increases, a mild peak emerges at $\phi = 0.16$, and then gradually decreases. For Al_2O_3 and TiO_2, Nu decreases monotonically as ϕ increases, and these two curves coincide almost indistinguishably. Therefore, these four curves display two distinct behaviors, namely, increasing monotonicity and decreasing monotonicity.

To describe mechanisms of these two distinct behaviors below, we choose Ag and TiO_2 nanofluid flows at $Ra = 10^4$. As shown in Fig. 4, the vertical velocity (Fig. 4(a), 4(c), and 4(e)) and the temperature (Fig. 4(b), 4(d), and 4(f)) of nanofluid flows at the mid-height position ($y = H/2$) versus x/H parameterized in concentration (ϕ) at $Ra = 10^4$ are presented. Because velocity curves in Figs. 4(a), 4(c), and 4(e) aggregate as ϕ increases, variations of the velocity can be hardly recognized. To overcome this difficulty, we show the maximum value of the vertical velocity (v_{max}) versus ϕ in inset figures in Figs. 4(a), 4(c), and 4(e), which clearly show the variation of velocity.

As shown in the inset of Fig. 4(a), for TiO_2 nanofluids at $AR = 1.5$, in the range of small ϕ values, v_{max} first increases as ϕ increases. It peaks at $\phi = 0.08$, and then reversely decreases as ϕ continues to increase. The trend in Fig. 4(a) shows that the convective strength of the nanofluid increases first and then decreases as ϕ continues to increase. It can be seen from Fig. 4(b) that the distortion of the temperature field is weakened and the temperature curve becomes straighter as ϕ increases, implying that the heat conduction continuously increases as ϕ increases. As illustrated from Figs. 4(a) and 4(b) above, for TiO_2 nanofluids at $AR = 1.5$, during $\phi < 0.08$, both the heat convection and the heat conduction are enhanced as ϕ increases, resulting in overall heat transfer increasing. However, during $\phi \geq 0.08$, the heat conduction enhances and the convection oppositely weakens as ϕ increases, but the enhancement of the heat conduction overwhelms the weakening of the heat convection, leading to the persisting heating trend of overall heat transfer.

As shown in the inset of Fig. 4(c), for TiO_2 nanofluids at $AR = 4$, v_{max} monotonously decreases as ϕ increases, suggesting that the flow convection weakens as ϕ increases. On the other hand, it can be seen from Fig. 4(d) that the temperature curve becomes straighter as ϕ increases, implying that the heat conduction enhances as ϕ increases. The trend of temperature curve variation resembles that in the case at $AR = 1.5$. As illustrated from Figs. 4(c) and 4(d) above, for TiO_2 nanofluids at $AR = 4$, the convection subsides and the heat conduction strengthens as ϕ increases. However, the weakening of the convection overwhelms the enhancement of the heat conduction, resulting in the deterioration of the overall heat transfer.

As shown in the inset of Fig. 4(e), for Ag nanofluids at $AR = 4$, in the range of large ϕ values, v_{max} increases as ϕ increases. It reaches the

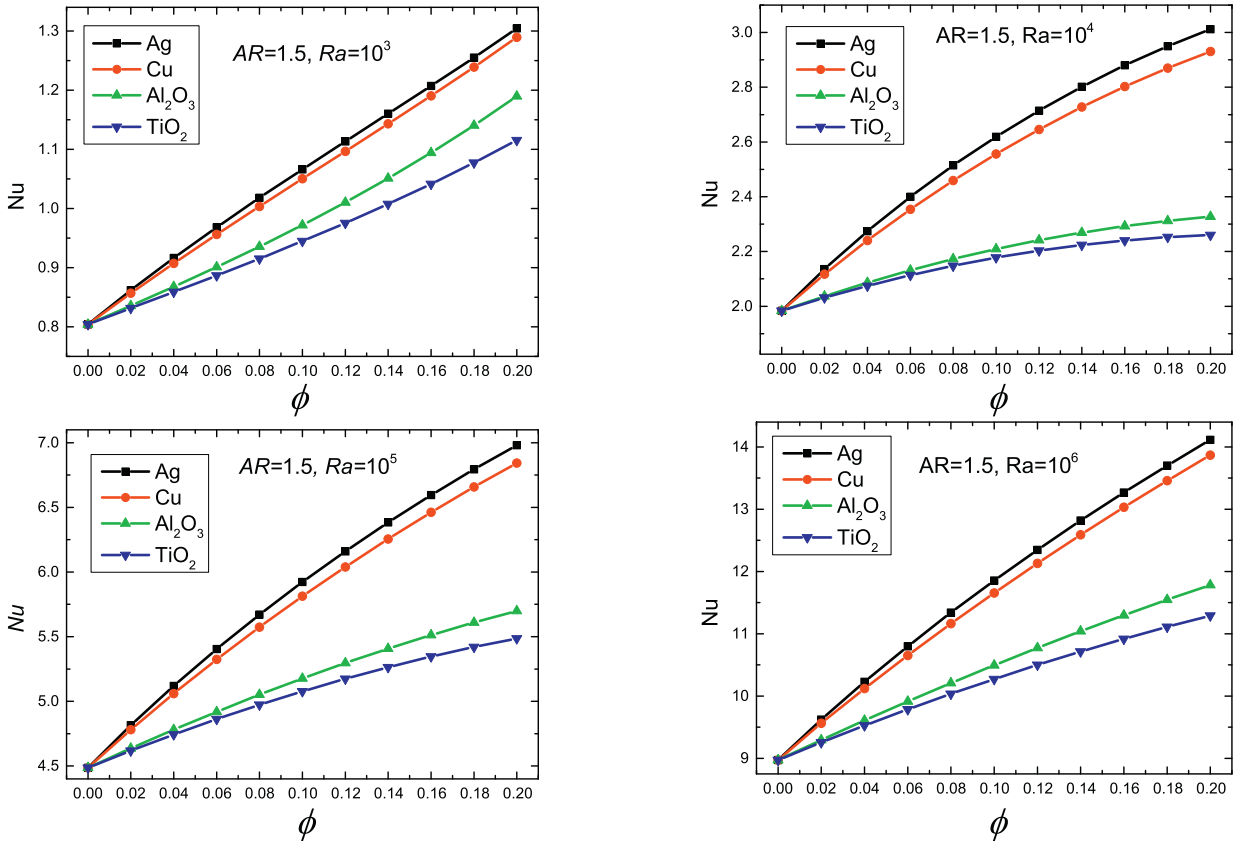

Fig. 2. Average Nusselt number (Nu) versus concentration (ϕ) of Ag, Cu, Al_2O_3, and TiO_2 nanofluids for $\phi = 0.0 \sim 0.20$ and various Rayleigh number (Ra) at $AR = 1.5$.

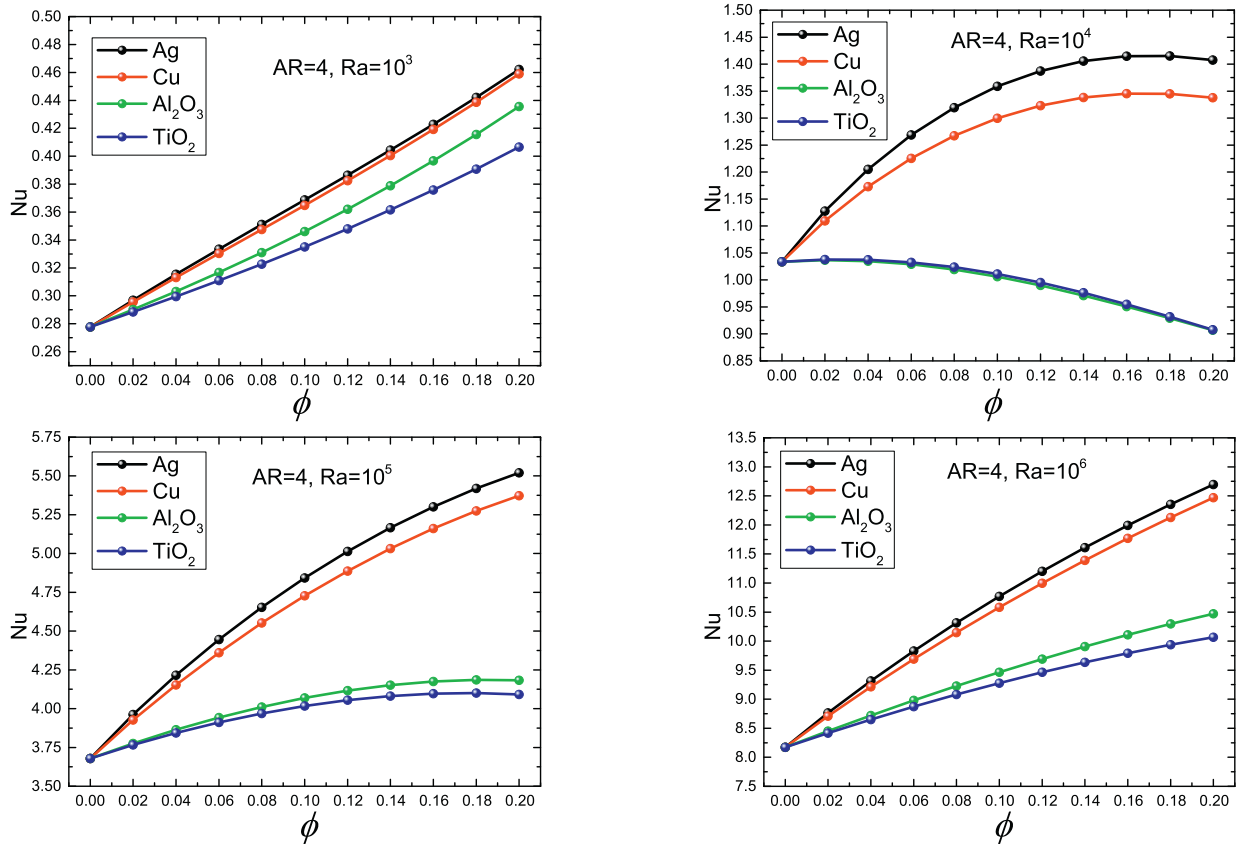

Fig. 3. Average Nusselt number (Nu) versus concentration (ϕ) of Ag, Cu, Al_2O_3, and TiO_2 nanofluids for $\phi = 0.0 \sim 0.20$ and various Rayleigh number (Ra) at $AR = 4$.

maximum at $\phi = 0.16$, and then reversely decreases as ϕ continues to increase. The trend of v_{max} curve means that the convective strength of the system increases first and then decreases with the increase of ϕ. It can be seen from Fig. 4(f) that the temperature distribution line becomes straighter as ϕ increases, which is similar to that of TiO_2 in Fig. 4(d). Nevertheless, the temperature distribution of Ag shows inconspicuously when it is compared with the case of TiO_2. As illustrated from Fig. 4(e) and 4(f) above, for Ag nanofluids at $AR = 4$, during $\phi < 0.16$, both the thermal convection and the thermal conduction are enhanced as ϕ increases, resulting in overall heat transfer increasing. During $\phi \geq 0.16$, the convection reversely weakens and the heat conduction strengthens as ϕ increases, but the weakening of heat convection surpasses the enhancement of heat conduction, leading to the fact that the overall heat transfer diminishes.

Variation trends of Cu nanofluids and Al_2O_3 nanofluids respectively resemble those of Ag nanofluids and TiO_2 nanofluids, and their descriptions are omitted here. As mentioned above, we have qualitatively described these heat transfer mechanisms of nanofluids at $Ra = 10^4$ in terms of velocity and temperature distributions of the nanofluids.

In order to further quantitatively explain the anomalous heat transfer behavior exhibited by nanofluids at $AR = 4$ and $Ra = 10^4$, we introduce and define accumulative conductive energy and convective energy as

$$Q_{cd} = \int_0^H \left(-k_{nf}\frac{\partial T}{\partial x}\right)\Big|_{x=L/2} dy \tag{17}$$

and

$$Q_{cv} = \int_0^H (u(\rho c_p)_{nf} T)\Big|_{x=L/2} dy, \tag{18}$$

both of two are post-processed at $x = L/2$. Because of the insulation on bottom and top walls, overall thermal energy must travel rightward. According to the law of energy conservation over the half-enclosure control volume, we obtain the total energy as

$$Q_T = Q_{cd} + Q_{cv}, \tag{19}$$

where

$$Q_T = \int_0^H \left(-k_{nf}\frac{\partial T}{\partial x}\right)\Big|_{x=0} dy. \tag{20}$$

According to the definition of Q_T, this quantity is mathematically proportional to Nu.

As shown in Fig. 5, we present the energy variation of these four types of nanofluids versus ϕ at $Ra = 10^4$ and $AR = 4$. For Cu, Ag, Al_2O_3, and TiO_2 nanofluids, all of the thermal conductive energy (Q_{cd}) monotonously increases as ϕ increases. However, for Cu nanofluids and Ag nanofluids, the dominant convective energy (Q_{cv}) first increases as ϕ increases. It maximizes at $\phi = 0.16$, and then decreases as ϕ continues to increase. In the range of $\phi < 0.16$, Q_{cv} and Q_{cd} increase with the increase of ϕ, leading to the increase of total energy Q_T. By contrast, in the range of $\phi \geq 0.16$, the dominant Q_{cv} begins to decreases as ϕ increases, causing Q_T mildly declines. For Al_2O_3 and TiO_2 nanofluids, Q_{cv} gradually decreases with the increase of ϕ, which is contrary to Q_{cd}. Because Q_{cv} dominates, Q_T monotonously decreases as ϕ increases. Consequently, Nu exhibits an anomalous decreasing heat transfer characteristic.

To investigate the mechanisms governing the effect of different Ra on nanofluids, we present three heat-transfer quantities (Q_T, Q_{cd}, Q_{cv}) versus at $Ra = 10^3$, 10^4, 10^5, and 10^6 for TiO_2 nanofluids and $AR = 4$ in Fig. 6. At $Ra = 10^3$, Q_{cd} dominates Q_{cv}, with the former monotonically increasing as ϕ increases. Even though Q_{cv} monotonously decreases as ϕ increases, but the variation of Q_{cv} is less than Q_{cd}. As a result, Q_T monotonically increases as ϕ increases. At $Ra = 10^4$, results has been mentioned in Fig. 5, and will be omitted here. At $Ra = 10^5$ and 10^6,

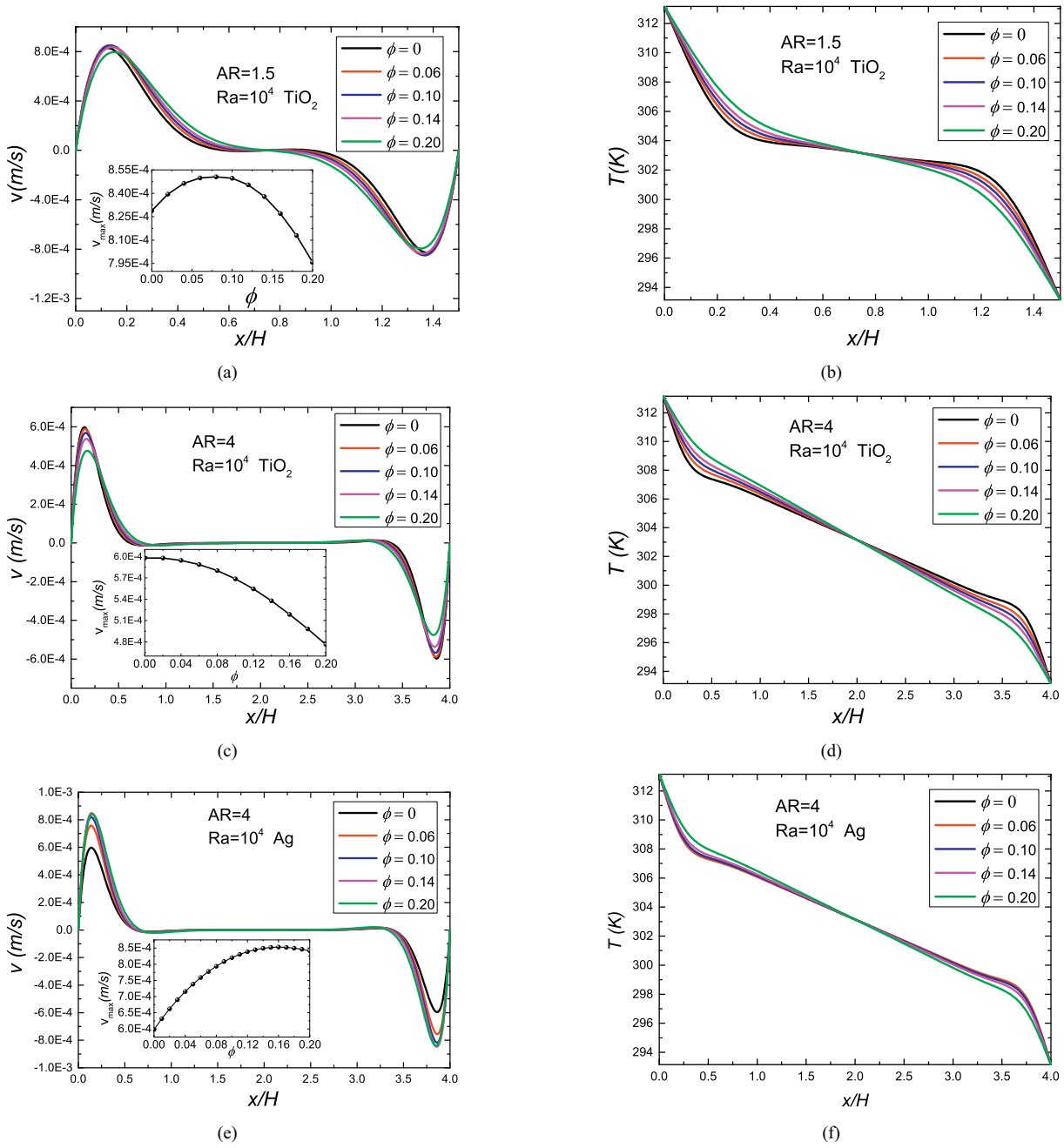

Fig. 4. Vertical velocity (v) and temperature (T) of nanofluid flows at the mid-height position ($y = H/2$) versus x/H parameterized in concentration (ϕ) at $Ra = 10^4$. (a)(c)(e) $v - x/H$. (b)(d)(f) $T - x/H$.

because of the insignificance of Q_{cd} value, and Q_{cv} dominance increases as ϕ increases, leading to the fact that Q_T monotonically increases as ϕ increases.

As mentioned in Fig. 2 and Fig. 3, the heat transfer shows different characteristics at different aspect ratio (AR). Herein, for the purpose of understanding effects of AR on the heat transfer characteristics, Nu values in enclosures for TiO_2 nanofluids parameterized by AR and ϕ at different Ra are presented in Fig. 7. At $Ra = 10^3$, Nu monotonically decreases as AR increases. In the entire range of $0 < \phi \leq 0.2$, at a fixed AR, Nu monotonically increases as ϕ increases. At $Ra = 10^4$, Nu also shows a monotonous decrease as AR increases. In addition, the critical AR value intersects at $AR \approx 2.5$, namely in the range of $AR < 2.5$, at a fixed AR, Nu monotonically increases as ϕ increases, whereas in the range of $AR \geq 2.5$, Nu exhibits decreasing as ϕ increases.

At $Ra = 10^5$ and a fixed ϕ, in the range of small aspect ratio values, Nu first decreases as AR increases. It arrives at the minimum, and then reversely increases as AR continues to increase. Reaching its local peak, it begins to decrease gradually, resembling a mildly zigzag trajectory, which was also discovered in pure-water results, reported in our previous work [50]. These local minima of zigzag trajectories are associated with the competition between thermal conduction and thermal convection, whereas local maxima of zigzag trajectories occur when the thermal convection dominates the overall thermal conduction (the thermal convection decreases as AR increases). On the other hand, in the range of $AR < 4.7$, zigzag heat transfer curves shift upward and rightward as ϕ increases. When AR approximately approaches 4.7, curves for and $\phi = 0.2$ intersect. In other words, in the range of $AR < 4.7$, at a fixed aspect ratio, Nu monotonically increases as ϕ increases. Beyond the intersection ($AR \geq 4.7$), at a fixed aspect ratio, the trend that Nu decreases as ϕ increases will occur.

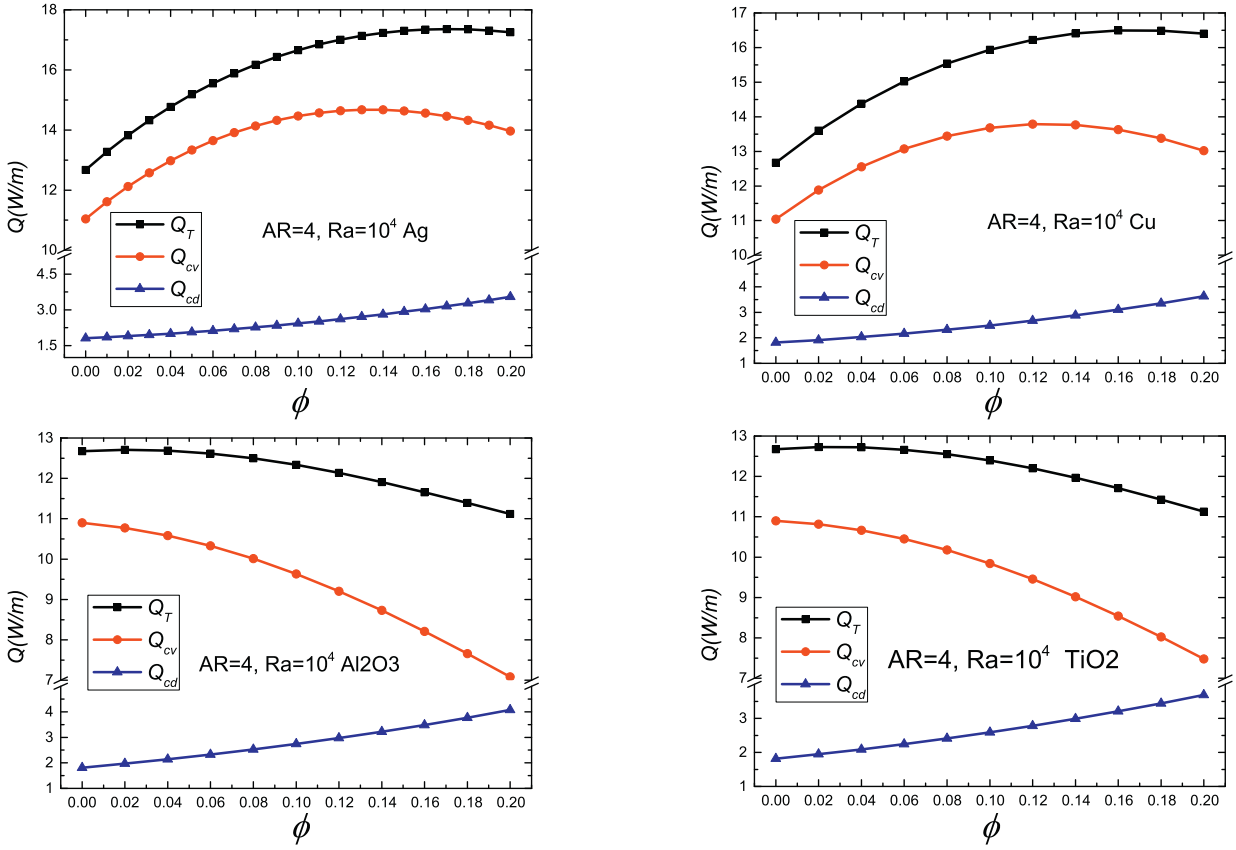

Fig. 5. Three heat-transfer quantities (Q_T, Q_{cd}, Q_{cv}) of four types nanofluid flows versus concentration (ϕ) at $Ra = 10^4$.

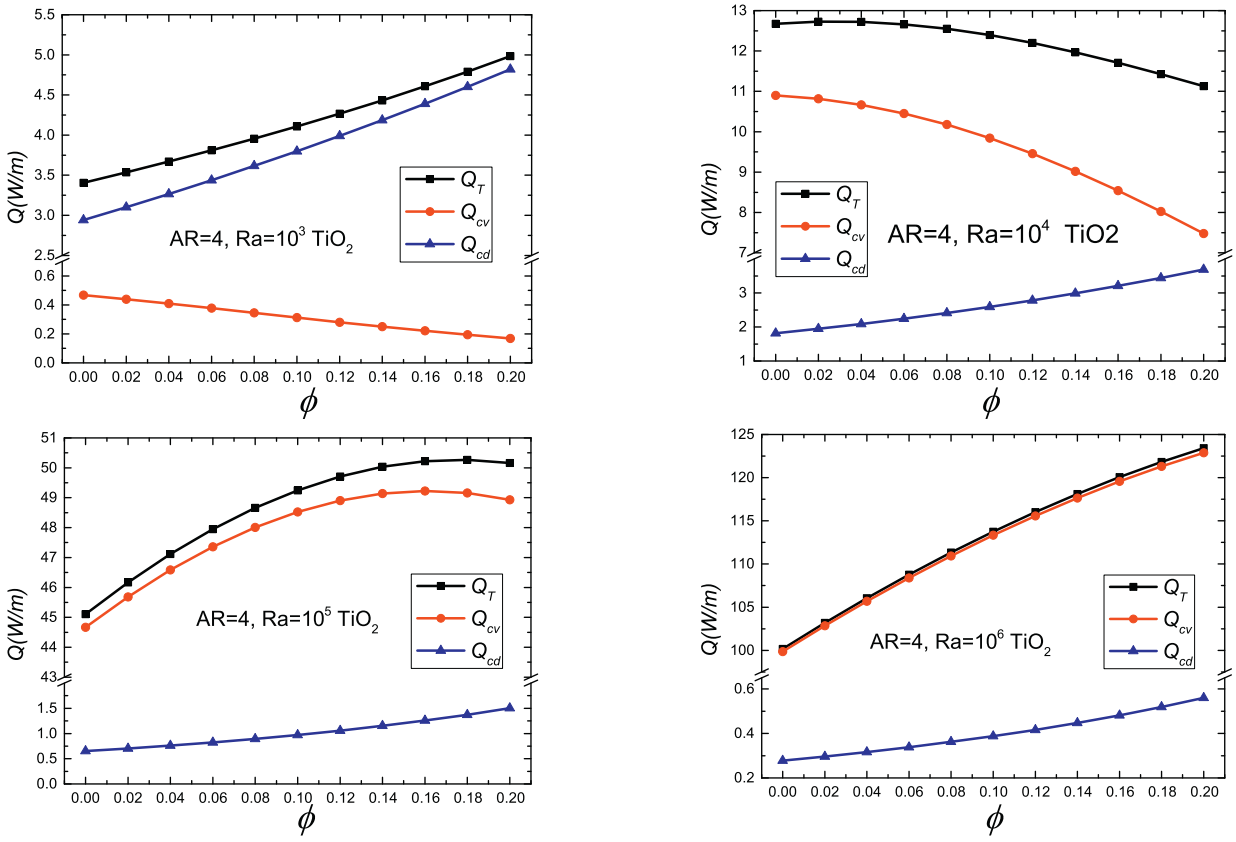

Fig. 6. Three heat-transfer quantities (Q_T, Q_{cd}, Q_{cv}) of TiO_2 nanofluid flows versus concentration (ϕ) at $Ra = 10^3$, 10^4, 10^5, and 10^6.

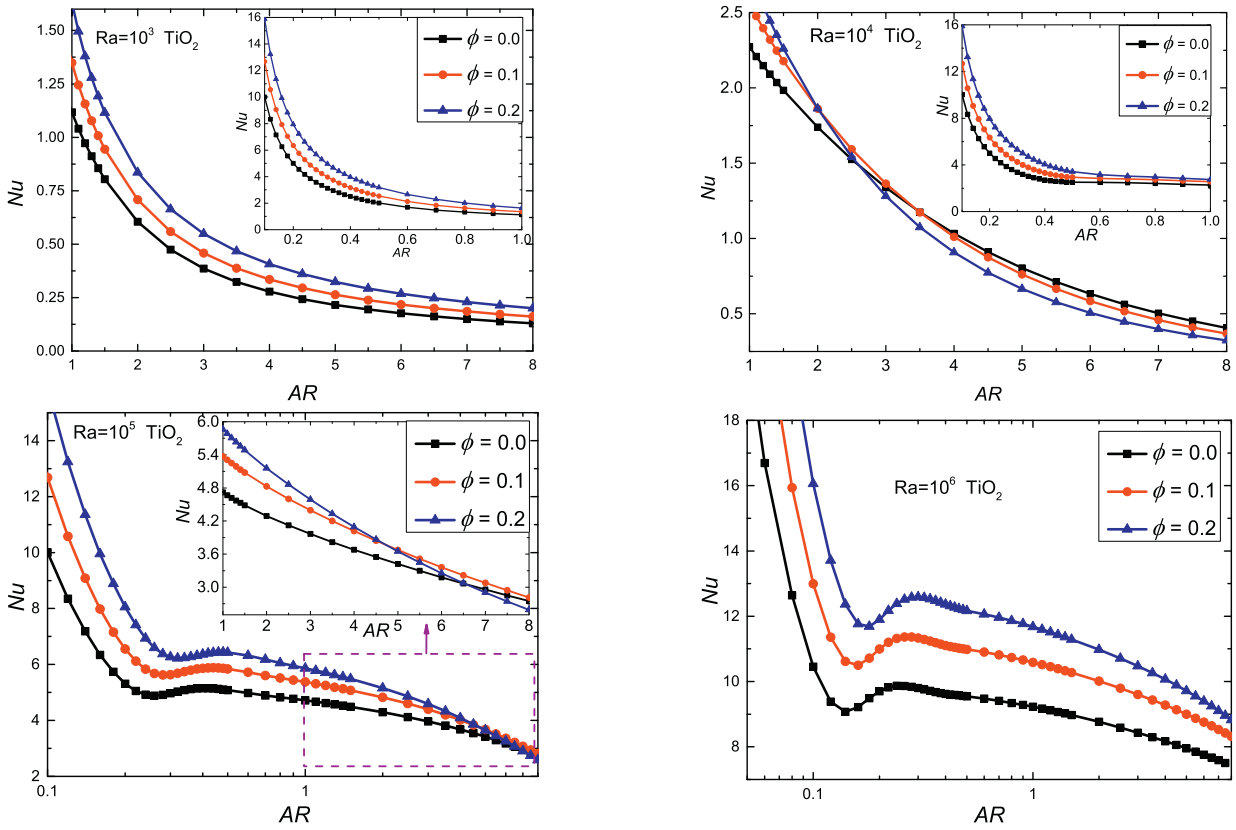

Fig. 7. Average Nusselt number (*Nu*) versus aspect ratio (*AR*) in enclosures with the TiO_2 nanofluid parameterized by concentration (ϕ) are presented at $Ra = 10^3 \sim 10^6$.

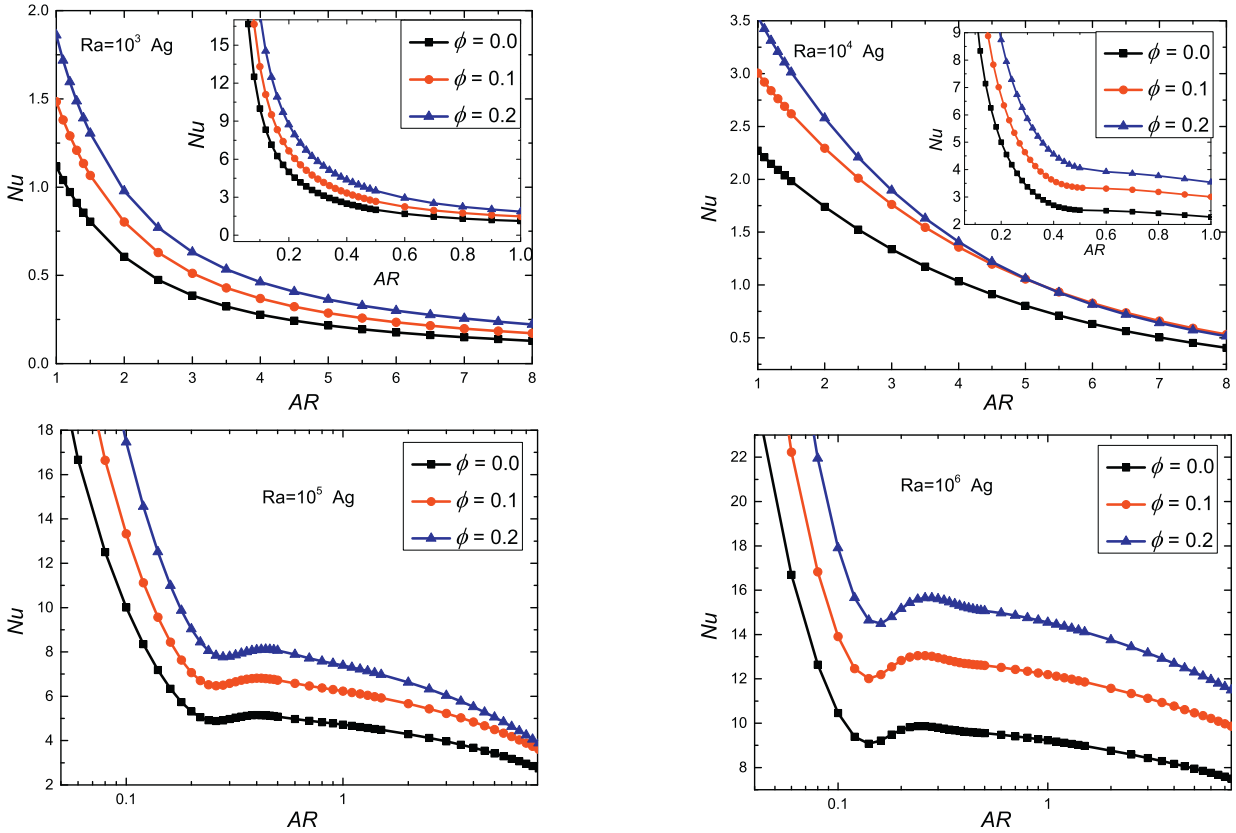

Fig. 8. Average Nusselt number (*Nu*) versus aspect ratio (*AR*) in enclosures with the *Ag* nanofluid parameterized by concentration (ϕ) are presented at $Ra = 10^3 \sim 10^6$.

At $Ra = 10^6$, at a fixed ϕ, the variation of zigzag pattern appears more conspicuous than that of $Ra = 10^5$ does. The difference lies in that, at a fixed aspect ratio, the intersection phenomenon will no longer take place, and Nu monotonically increases as ϕ increases. As illustrated from Fig. 7 at $Ra = 10^5$ and 10^6 above, the zigzag pattern of the local maximum positions and the local minimum positions can be applied to designs pertaining to either maximal insulation or maximal cooling.

Finally for the purpose of comparisons, Nu values in enclosures for Ag nanofluids parameterized by AR and ϕ at different Ra are presented in Fig. 8. At $Ra = 10^3 \sim 10^6$, heat transfer characteristics of Ag nanofluids look similar to those of TiO_2 nanofluids. However, for Ag nanofluids at $Ra = 10^4$ the critical AR value rightward intersects at $AR \approx 5.3$, namely, at a fixed AR, when $AR < 5.3$, Nu increases as ϕ increases. For $AR \geq 5.3$, the trend that Nu decrease as ϕ increases will occur. For Ag nanofluids at $Ra = 10^5$, the critical AR value shifts rightward and the intersection vanishes in the range of $0 < AR \leq 8$.

5. Conclusion

The present study offers our finding, in which the heat transfer of the circulating nanofluid flow within rectangular enclosures may increase or decrease as the nanoparticle volume concentration increases. The vertical velocity distribution and the temperature distribution at the mid-height of the enclosure are used to qualitatively estimate these mechanisms. Subsequently, we utilize three heat-transfer quantities (Q_T, Q_{cd}, Q_{cv}) to quantitatively describe governing mechanisms. Furthermore, the critical aspect ratio of these two opposite phenomena is presented. It is also discovered that Nusselt number exhibits a mildly zigzag pattern when aspect ratio varies at large Rayleigh numbers. Our investigation may shed light on various thermal-engineering-system designs that aim at either enhancing or attenuating the heat transfer.

Credit author statement

Bin Wang: Conceptualization, Methodology, Investigation, Software, Validation, Data curation, Visualization, Writing- Original draft preparation, Writing- Reviewing and Editing, Funding acquisition.

Tien-Mo Shih: Writing- Original draft preparation, Writing- Reviewing and Editing, Supervision.

Jiping Huang: Supervision, Funding acquisition.

Declaration of Competing Interest

None.

Acknowledgments

This work is supported by China Postdoctoral Science Foundation under Grant No. 2019M661354 and by National Natural Science Foundation of China under Grant No. 11725521.

References

[1] H. Türkoglu, N. Yücel, Effect of heater and cooler locations on natural convection in square cavities, Numerical Heat Transfer, Part A: Applications 27 (3) (1995) 351–358.
[2] J.H. Bae, J.M. Hyun, Time-dependent buoyant convection in an enclosure with discrete heat sources, Int. J. Therm. Sci. 43 (1) (2004) 3–11.
[3] M.A. Sharif, T.R. Mohammad, Natural convection in cavities with constant flux heating at the bottom wall and isothermal cooling from the sidewalls, Int. J. Therm. Sci. 44 (9) (2005) 865–878.
[4] B. Calcagni, F. Marsili, M. Paroncini, Natural convective heat transfer in square enclosures heated from below, Appl. Therm. Eng. 25 (16) (2005) 2522–2531.
[5] A.K. Sharma, K. Velusamy, C. Balaji, Turbulent natural convection in an enclosure with localized heating from below, Int. J. Therm. Sci. 46 (12) (2007) 1232–1241.
[6] S.U.S. Choi, J. Eastman, Enhancing thermal conductivity of fluids with nanoparticles, ASME-Publications-Fed 231 (1995) 99–106.
[7] S. Lee, S.U.S. Choi, Application of metallic nanoparticle suspensions in advanced cooling systems, Tech. rep., Argonne National Lab., IL (United States) (1996).
[8] S. Lee, S.U.S. Choi, S. Li, J. Eastman, Measuring thermal conductivity of fluids containing oxide nanoparticles, J. Heat Transf. 121 (2) (1999) 280–289.
[9] J. Eastman, S.U.S. Choi, S. Li, W. Yu, L. Thompson, Anomalously increased effective thermal conductivities of ethylene glycol-based nanofluids containing copper nanoparticles, Appl. Phys. Lett. 78 (6) (2001) 718–720.
[10] Y. Xuan, Q. Li, Heat transfer enhancement of nanofluids, Int. J. Heat Fluid Flow 21 (1) (2000) 58–64.
[11] E. Abu-Nada, H.F. Oztop, Effects of inclination angle on natural convection in enclosures filled with cu–water nanofluid, Int. J. Heat Fluid Flow 30 (4) (2009) 669–678.
[12] N.C. Roy, Natural convection of nanofluids in a square enclosure with different shapes of inner geometry, Phys. Fluids 30 (11) (2018) 113605.
[13] M.A. Nazari, R. Ghasempour, M.H. Ahmadi, G. Heydarian, M.B. Shafi-i, Experimental investigation of graphene oxide nanofluid on heat transfer enhancement of pulsating heat pipe, Int. Comm. Heat and Mass Transf. 91 (2018) 90–94.
[14] R. Lotfi, Y. Saboohi, A. Rashidi, Numerical study of forced convective heat transfer of nanofluids: comparison of different approaches, Int. Comm. Heat and Mass Transf. 37 (1) (2010) 74–78.
[15] S.Z. Heris, S.G. Etemad, M.N. Esfahany, Experimental investigation of oxide nanofluids laminar flow convective heat transfer, Int. Comm. Heat and Mass Transf. 33 (4) (2006) 529–535.
[16] X. Wang, X. Li, Y. Xu, D. Zhu, Thermal energy storage characteristics of Cu-H_2O nanofluids, Energy 78 (2014) 212–217.
[17] K. Khanafer, K. Vafai, M. Lightstone, Buoyancy-driven heat transfer enhancement in a two-dimensional enclosure utilizing nanofluids, Int. J. Heat Mass Transf. 46 (19) (2003) 3639–3653.
[18] R.-Y. Jou, S.-C. Tzeng, Numerical research of nature convective heat transfer enhancement filled with nanofluids in rectangular enclosures, Int. Comm. Heat and Mass Transf. 33 (6) (2006) 727–736.
[19] C.-J. Ho, M. Chen, Z. Li, Numerical simulation of natural convection of nanofluid in a square enclosure: effects due to uncertainties of viscosity and thermal conductivity, Int. J. Heat Mass Transf. 51 (17) (2008) 4506–4516.
[20] H.F. Oztop, E. Abu-Nada, Numerical study of natural convection in partially heated rectangular enclosures filled with nanofluids, Int. J. Heat Fluid Flow 29 (5) (2008) 1326–1336.
[21] E.B. Öğüt, Natural convection of water-based nanofluids in an inclined enclosure with a heat source, Int. J. Therm. Sci. 48 (11) (2009) 2063–2073.
[22] G. Sheikhzadeh, A. Arefmanesh, M. Kheirkhah, R. Abdollahi, Natural convection of cu–water nanofluid in a cavity with partially active side walls, Eur. J. Mech.-B/Fluids 30 (2) (2011) 166–176.
[23] S. Kumar, S.K. Prasad, J. Banerjee, Analysis of flow and thermal field in nanofluid using a single phase thermal dispersion model, Appl. Math. Model. 34 (3) (2010) 573–592.
[24] M. Saïdi, G. Karimi, Free convection cooling in modified L-shape enclosures using copper–water nanofluid, Energy 70 (2014) 251–271.
[25] N. Putra, W. Roetzel, S.K. Das, Natural convection of nano-fluids, Heat Mass Transf. 39 (8–9) (2003) 775–784.
[26] A.K. Santra, S. Sen, N. Chakraborty, Study of heat transfer augmentation in a differentially heated square cavity using copper–water nanofluid, Int. J. Therm. Sci. 47 (9) (2008) 1113–1122.
[27] K.C. Lin, A. Violi, Natural convection heat transfer of nanofluids in a vertical cavity: effects of non-uniform particle diameter and temperature on thermal conductivity, Int. J. Heat Fluid Flow 31 (2) (2010) 236–245.
[28] G.A. Sheikhzadeh, A. Arefmanesh, M. Mahmoodi, Numerical study of natural convection in a differentially-heated rectangular cavity filled with TiO_2-water nanofluid, J. Nano Res. Vol. 13 (2011) 75–80. Trans Tech Publ.
[29] C.H. Chon, K.D. Kihm, S.P. Lee, S.U. Choi, Empirical correlation finding the role of temperature and particle size for nanofluid (Al_2O_3) thermal conductivity enhancement, Appl. Phys. Lett. 87 (15) (2005) 153107.
[30] C. Nguyen, F. Desgranges, G. Roy, N. Galanis, T. Mare, S. Boucher, H.A. Mintsa, Temperature and particle-size dependent viscosity data for water-based nanofluids–hysteresis phenomenon, Int. J. Heat Fluid Flow 28 (6) (2007) 1492–1506.
[31] E. Abu-Nada, Z. Masoud, H.F. Oztop, A. Campo, Effect of nanofluid variable properties on natural convection in enclosures, Int. J. Therm. Sci. 49 (3) (2010) 479–491.
[32] H. Brinkman, The viscosity of concentrated suspensions and solutions, J. Chem. Phys. 20 (4) (1952) 571.
[33] J. C. Maxwell, A treatise on electricity and magnetism, Vol. 1, Clarendon press, 1881.
[34] D. Wen, Y. Ding, Experimental investigation into convective heat transfer of nanofluids at the entrance region under laminar flow conditions, Int. J. Heat Mass Transf. 47 (24) (2004) 5181–5188.
[35] H.F. Öztop, P. Estellé, W.-M. Yan, K. Al-Salem, J. Orfi, O. Mahian, A brief review of natural convection in enclosures under localized heating with and without nanofluids, Int. Comm. Heat and Mass Transf. 60 (2015) 37–44.
[36] K. Solangi, S. Kazi, M. Luhur, A. Badarudin, A. Amiri, R. Sadri, M. Zubir, S. Gharehkhani, K. Teng, A comprehensive review of thermophysical properties and convective heat transfer to nanofluids, Energy 89 (2015) 1065–1086.
[37] L. Yang, K. Du, A comprehensive review on heat transfer characteristics of TiO_2 nanofluids, Int. J. Heat Mass Transf. 108 (2017) 11–31.
[38] R. Ganvir, P. Walke, V. Kriplani, Heat transfer characteristics in nanofluidła review, Renew. Sust. Energ. Rev. 75 (2017) 451–460.
[39] B. Ghasemi, S. Aminossadati, Brownian motion of nanoparticles in a triangular enclosure with natural convection, Int. J. Therm. Sci. 49 (6) (2010) 931–940.
[40] M. Mahmoodi, Numerical simulation of free convection of a nanofluid in L-shaped cavities, Int. J. Therm. Sci. 50 (9) (2011) 1731–1740.

[41] E. Abu-Nada, Z. Masoud, A. Hijazi, Natural convection heat transfer enhancement in horizontal concentric annuli using nanofluids, Int. Comm. Heat and Mass Transf. 35 (5) (2008) 657–665.
[42] I. Ishihara, T. Fukui, R. Matsumoto, Natural convection in a vertical rectangular enclosure with symmetrically localized heating and cooling zones, Int. J. Heat Fluid Flow 23 (3) (2002) 366–372.
[43] G. de Vahl Davis, Natural convection of air in a square cavity: a bench mark numerical solution, Int. J. Numer. Methods Fluids 3 (3) (1983) 249–264.
[44] G. Barakos, E. Mitsoulis, D. Assimacopoulos, Natural convection flow in a square cavity revisited: laminar and turbulent models with wall functions, Int. J. Numer. Methods Fluids 18 (7) (1994) 695–719.
[45] T. Fusegi, J. Hyun, K. Kuwahara, B. Farouk, A numerical study of three-dimensional natural convection in a differentially heated cubical enclosure, Int. J. Heat Mass Transf. 34 (6) (1991) 1543–1557.
[46] COMSOL Multiphysics User"s Guide (Version 4.3 a), COMSOL AB, (2012).
[47] B.G. Galerkin, Series solution of some problems of elastic equilibrium of rods and plates, Vestn. Inzh. Tekh 19 (1915) 897–908.
[48] T.M. Shih, Numerical Heat Transfer, Springer-Verlag, New York, 1984.
[49] B. Wang, T.-M. Shih, C.-X. Wu, Characteristics of instantaneous heat transfer rates in three heat-transfer-coefficient regimes, Int. J. Heat Mass Transf. 93 (2016) 889–895.
[50] B. Wang, T.-M. Shih, B. Tian, C.-X. Wu, R.R.-G. Chang, Mildly zigzag heat transfer affected by aspect ratios for recirculating flows in rectangular enclosures, Int. J. Heat Mass Transf. 107 (2017) 372–378.